Accounting for canopy structure improves hyperspectral radiative transfer and sun-induced chlorophyll fluorescence representations in a new generation Earth System model

Renato K. Braghiere[1,2*], Yujie Wang[3], Russell Doughty[3], Daniel Sousa[1], Troy Magney[4], Jean-Luc Widlowski[5], Marcos Longo[1], A. Anthony Bloom[1], John Worden[1], Pierre Gentine[6], Christian Frankenberg[1,3]

[1] Jet Propulsion Laboratory, California Institute of Technology, 4800 Oak Grove Drive, Pasadena, CA, 91109 USA

[2] Joint Institute for Regional Earth System Science and Engineering, University of California at Los Angeles, Los Angeles, CA, 90095 USA

[3] Division of Geological and Planetary Sciences, California Institute of Technology, Pasadena, CA 91125

[4] Department of Plant Sciences, University of California, Davis, CA, USA

[5] European Commission-DG Joint Research Centre, Institute for Environment and Sustainability, Ispra, VA I-21027, Italy

[6] Department of Earth and Environmental Engineering, Columbia University, New York, New York, 10027 USA

[*]Corresponding author: Dr. Renato K. Braghiere (renato.k.braghiere@jpl.nasa.gov)

Current address: NASA Jet Propulsion Laboratory, M/S 233–305F, 4800 Oak Grove Drive, Pasadena, CA 91109, USA.

Supplemental material

A RAMI4PILPS benchmarking examples: broadband PAR and NIR

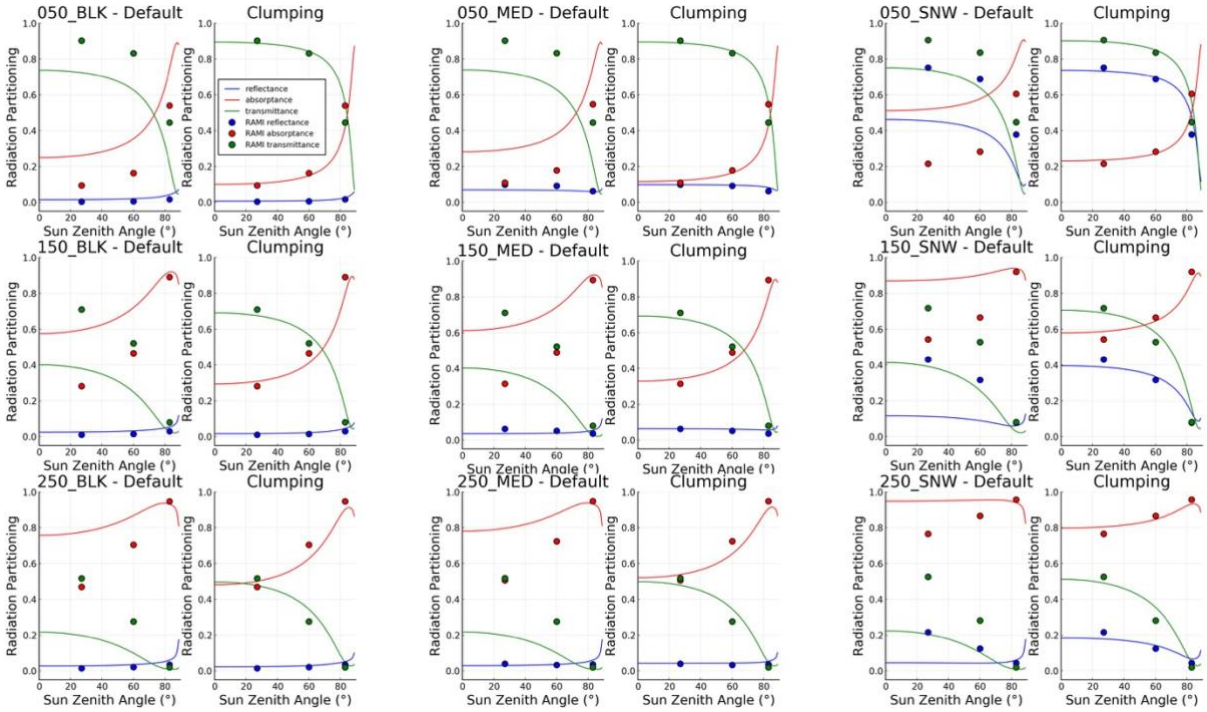

Figure S1. Intercomparison of zenith profile of the fraction of direct absorbed (red), reflected (blue), and transmitted (green) for PAR (400-700 nm) calculated with 2 different model setups with (clumping) and without clumping (default) for three different LAI values: 0.5 $m^2.m^{-2}$, 1.5 $m^2.m^{-2}$, 2.5 $m^2.m^{-2}$, and three different soil albedos: BLK (black; $\alpha_{soil} = 0.00$), MED (medium; $\alpha_{soil} = 0.12$), and SNW (snow; $\alpha_{soil} = 0.96$). The RAMI4PILPS reference values obtained with a 3D Monte Carlo ray-tracing model, raytran, are indicated by points.

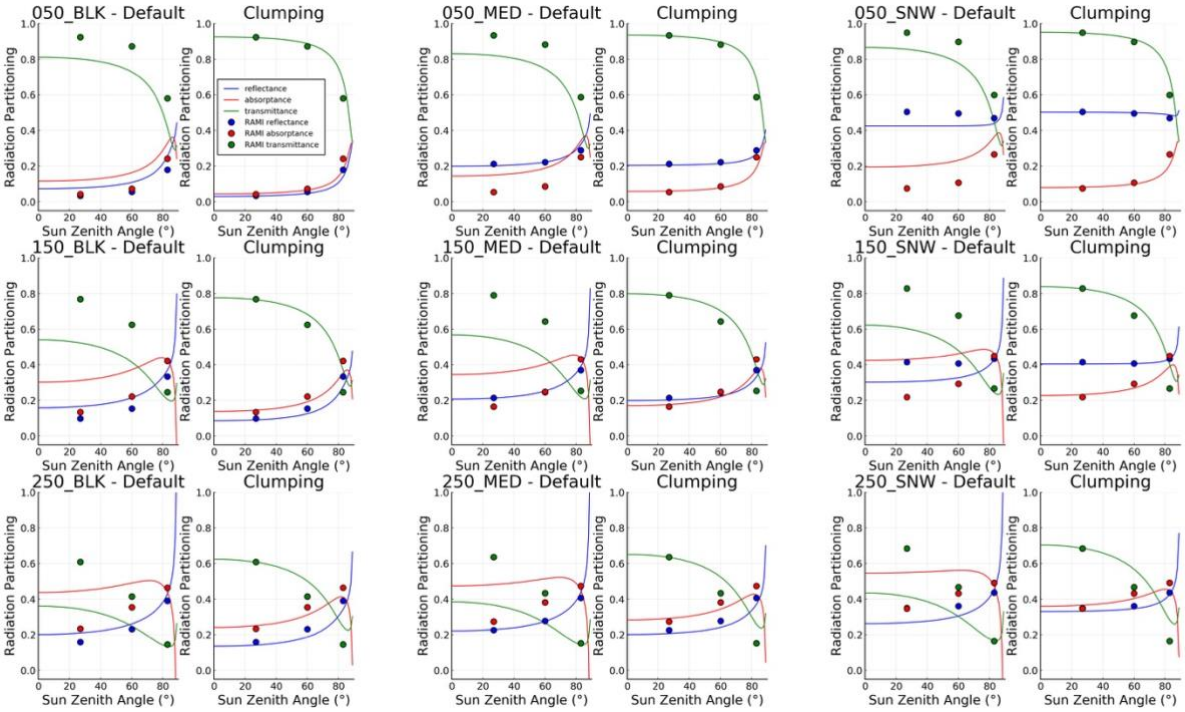

Figure S2. Intercomparison of zenith profile of the fraction of direct absorbed (red), reflected (blue), and transmitted (green) for NIR (700-2500 nm) calculated with 2 different model setups with (clumping) and without clumping (default) for three different LAI values: 0.5 $m^2.m^{-2}$, 1.5 $m^2.m^{-2}$, 2.5 $m^2.m^{-2}$, and three different soil albedos: BLK (black; $\alpha_{soil} = 0.00$), MED (medium; $\alpha_{soil} = 0.21$), and SNW (snow; $\alpha_{soil} = 0.56$). The RAMI4PILPS reference values obtained with a 3D Monte Carlo ray-tracing model, raytran, are indicated by points.

B RAMI4PILPS benchmarking examples: broadband PAR and NIR

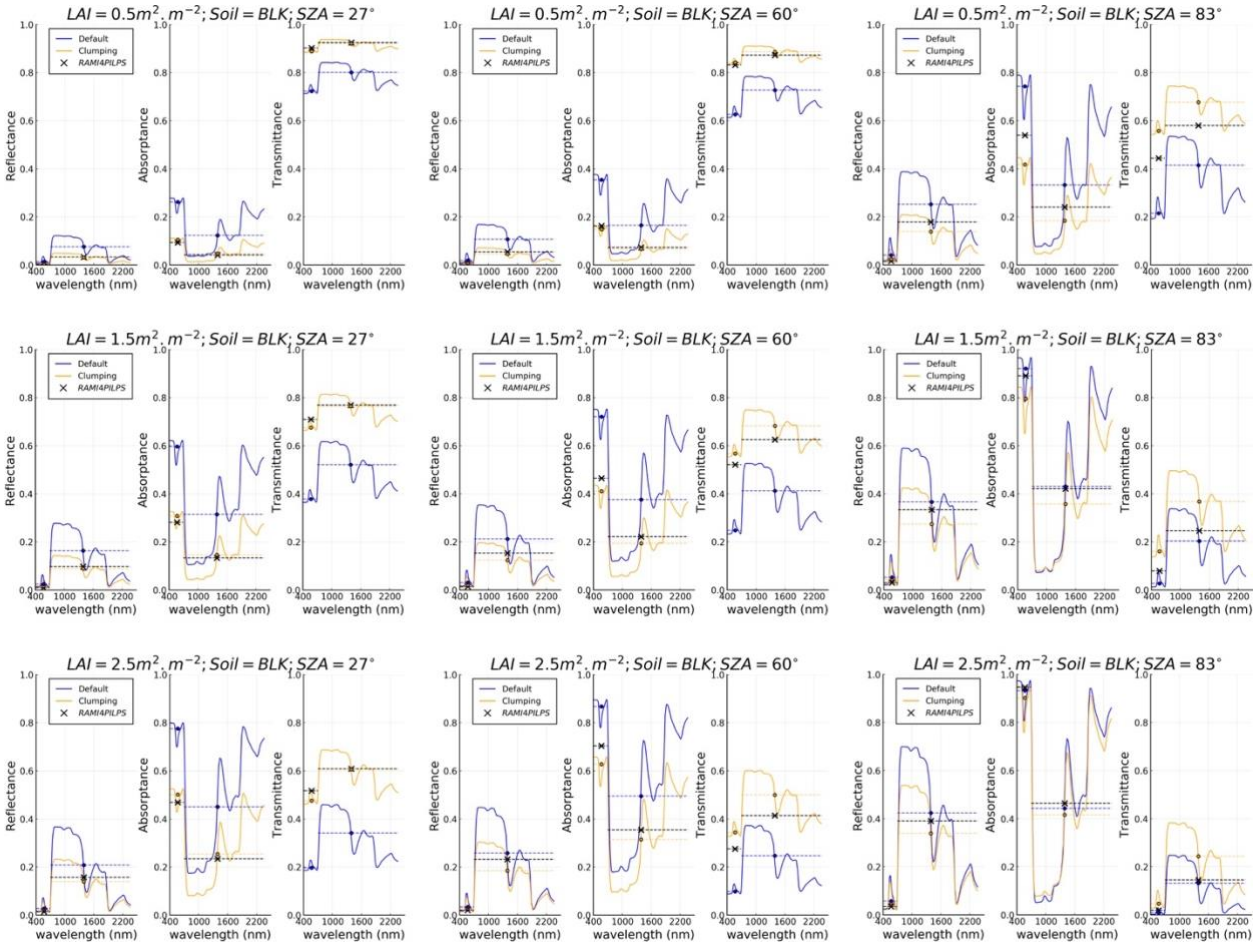

Figure S3. Intercomparison of the fraction of direct hyperspectral absorbed, reflected, and transmitted shortwave radiation (400-2500 nm) calculated with 2 different model setups with (clumping) and without clumping (default) for three different LAI values: 0.5 $m^2.m^{-2}$, 1.5 $m^2.m^{-2}$, 2.5 $m^2.m^{-2}$, a black soil albedo BLK (black; $\alpha_{soil} = 0.00$), and three sun zenith angles: 27°, 60°, and 83°. The RAMI4PILPS reference values obtained with a 3D Monte Carlo ray-tracing model, raytran, are indicated by points.

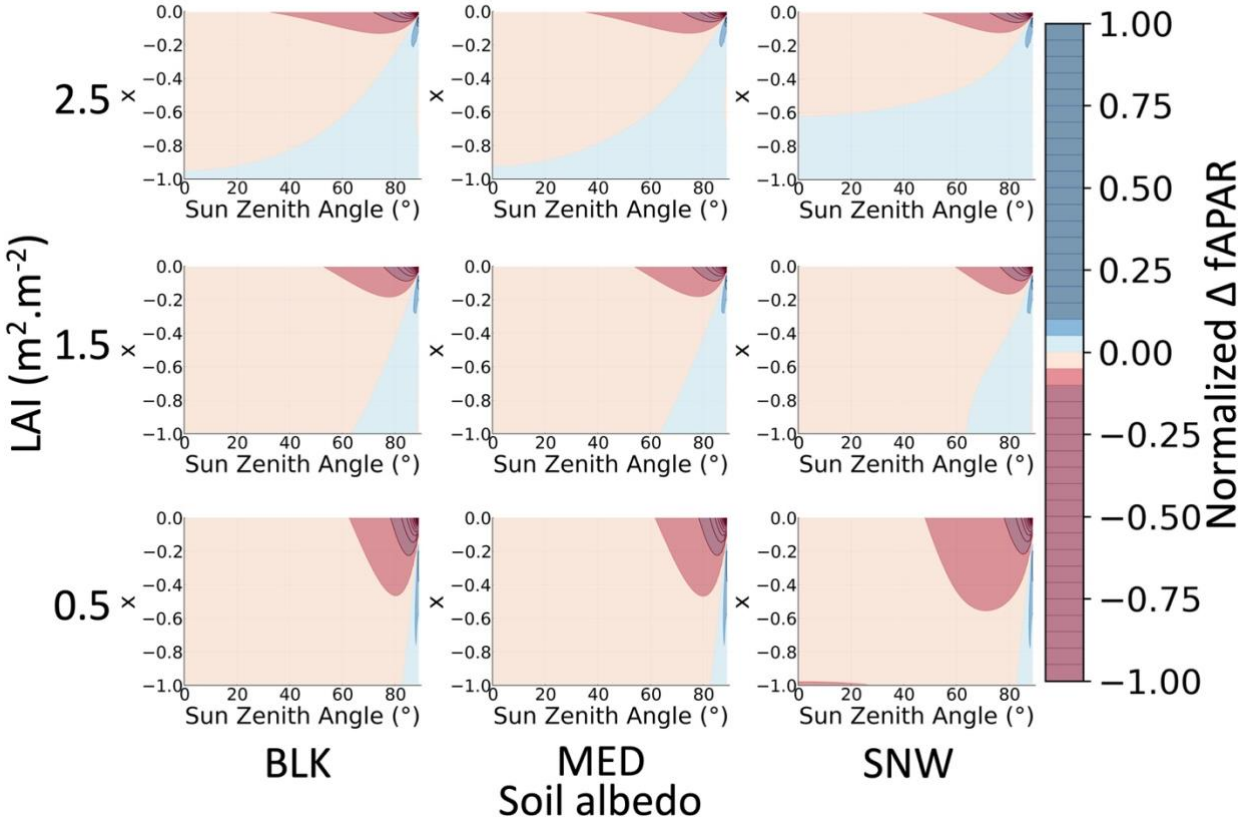

Figure S4. Vertical zenith profile of normalized fAPAR difference between the modified CliMA-Land RT with clumping index minus the non-clump version for 3 canopy densities (0.5, 1.5, and 2.5 $m^2.m^{-2}$) over 3 soil albedos (BLK, MED, SNW). x is the relative optical height, which runs from −1 at the bottom to zero at the top of canopy.

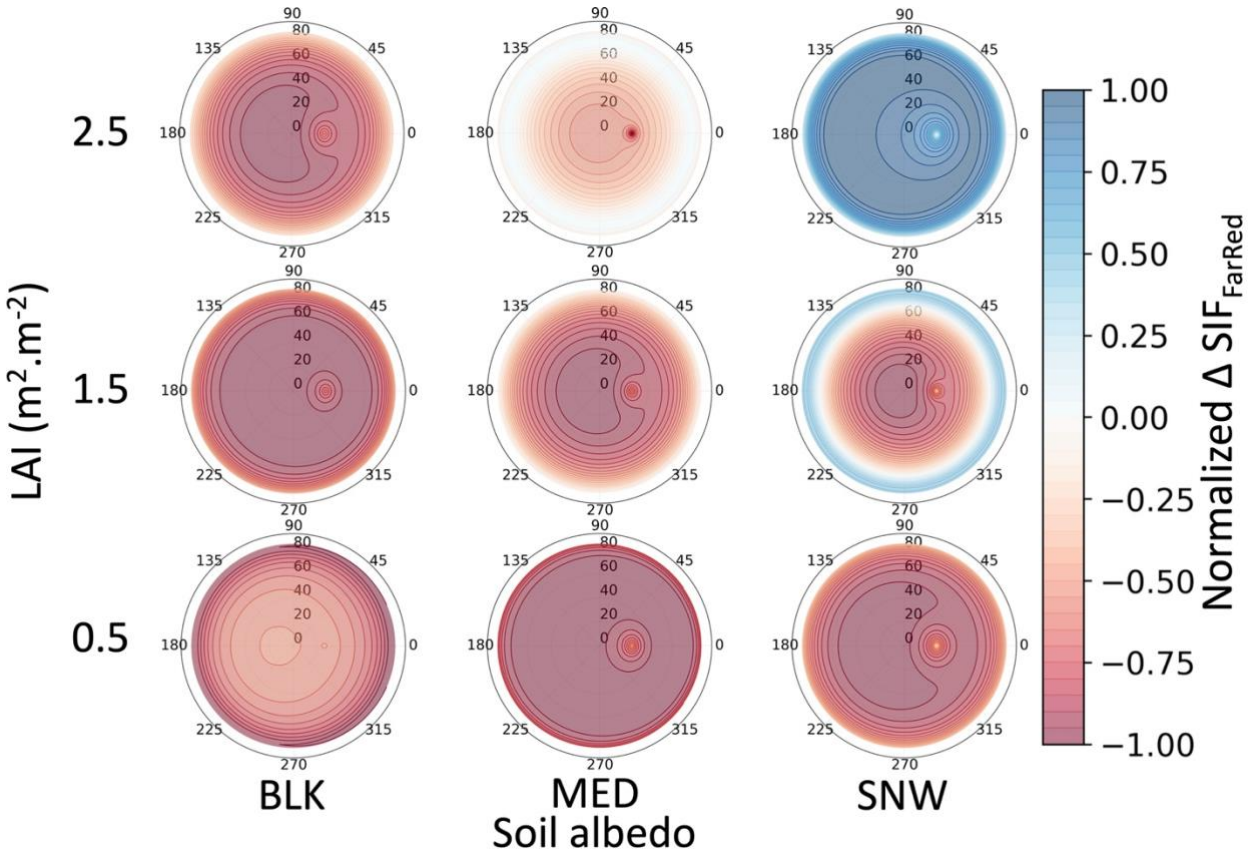

Figure S5. Polar plot of normalized SIF_{FarRed} difference between the modified CliMA-Land RT with clumping index minus the non-clumped version for 3 canopy densities (0.5, 1.5, and 2.5 $m^2.m^{-2}$) over 3 soil albedos (BLK, MED, SNW) with sun zenith angle at 27 degrees. The radial axis corresponds to the view zenith angle in degrees and the angular axis corresponds to the relative azimuth in degrees.

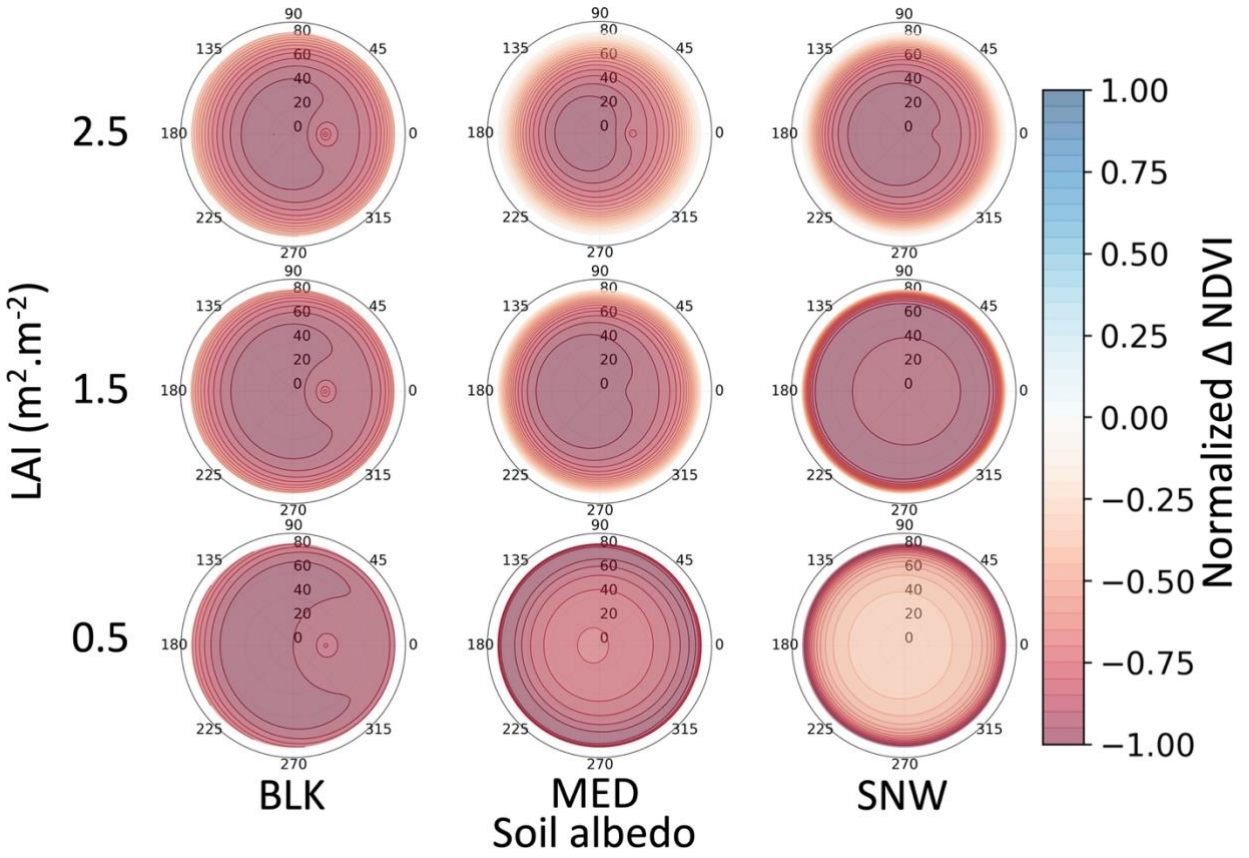

Figure S6. Polar plot of normalized NDVI difference between the modified CliMA-Land RT with clumping index minus the non-clumped version for 3 canopy densities (0.5, 1.5, and 2.5 $m^2.m^{-2}$) over 3 soil albedos (BLK, MED, SNW) with sun zenith angle at 27 degrees. The radial axis corresponds to the view zenith angle in degrees and the angular axis corresponds to the relative azimuth in degrees.

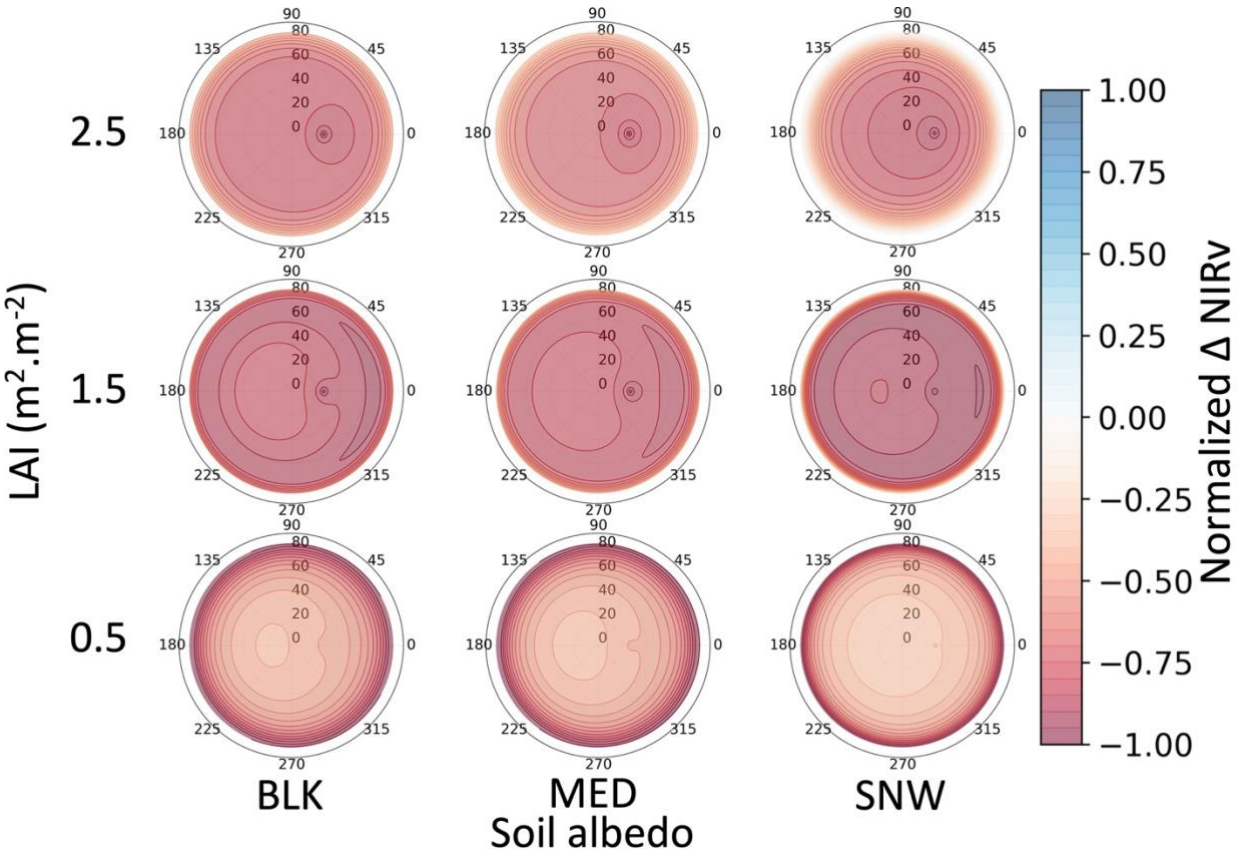

Figure S7. Polar plot of normalized NIRv difference between the modified CliMA-Land RT with clumping index minus the non-clumped version for 3 canopy densities (0.5, 1.5, and 2.5 $m^2.m^{-2}$) over 3 soil albedos (BLK, MED, SNW) with sun zenith angle at 27 degrees. The radial axis corresponds to the view zenith angle in degrees and the angular axis corresponds to the relative azimuth in degrees.

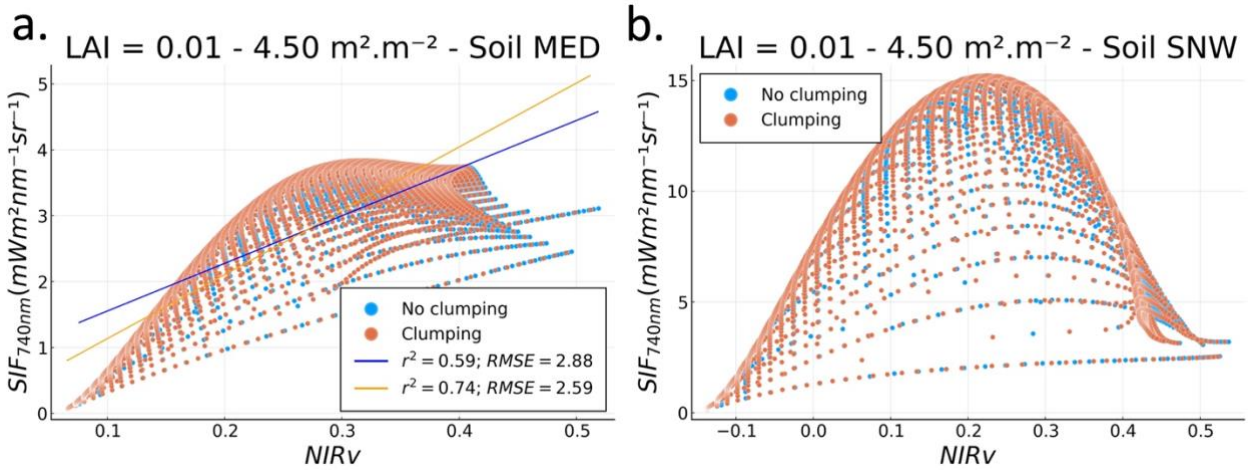

Figure S8. Linear fit between SIF_{740nm} and NIR_v for the modified CliMA-Land radiative transfer with clumping index and the default version for multiple canopy densities (from LAI = 0.01 $m^2.m^{-2}$ to LAI = 4.50 $m^2.m^{-2}$) over **a.** a medium soil albedo (MED), and **b.** a snowy soil albedo (SNW) with clumping calculate through **Eq.(2)** for sun zenith angles from 0° to 89°,

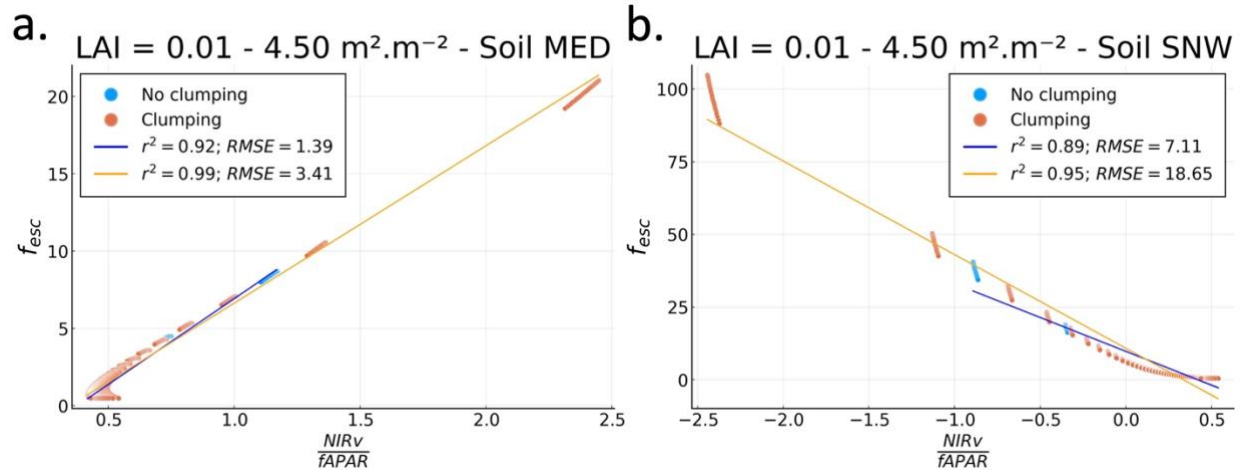

Figure S9. Linear fit between the fluorescence scape ratio (f_{esc}) and the NIR_v/fAPAR for the modified CliMA-Land radiative transfer with clumping index and the default version for multiple canopy densities and over **a.** a medium soil albedo (MED), and b. a snowy soil albedo (SNW) with clumping calculate through **Eq.(2)** for sun zenith angles from 0° to 30°.

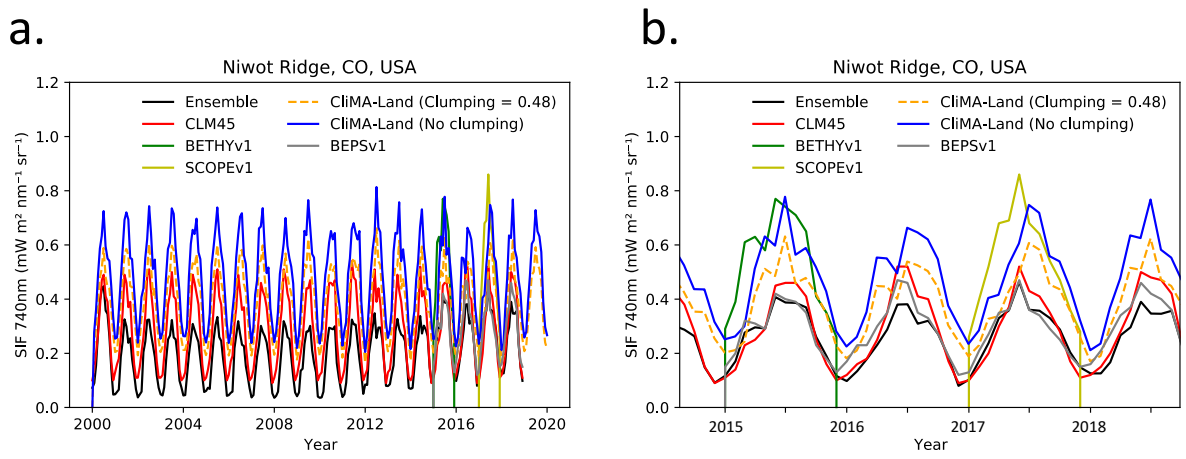

Figure S10. Simulated yearly cycles of SIF at 740 nm (mW m^{-2} nm^{-1} sr^{-1}) for Niwot Ridge, CO, USA from **a.** 2000 to 2018 and **b.** from 2015 to 2018. The across-model average (i.e., "Ensemble" represented by a black line) represents the average of all model scenarios (SiB3, SiB3-LAI, SiB4, Orchv1 (temp stress), Orchv2 (water stress), Orchv3 (temp stress, OCO-2 Opt), BEPSv1, BEPSv2, CLM45, CLM50v1, CLM50v2, CLM50v3, BETHYv1, BETHYv2, BETHYv3, SCOPEv1, and SCOPEv2). The summary of all SIF models and within-model experiments illustrating model components are described in Parazoo et al., (2020).

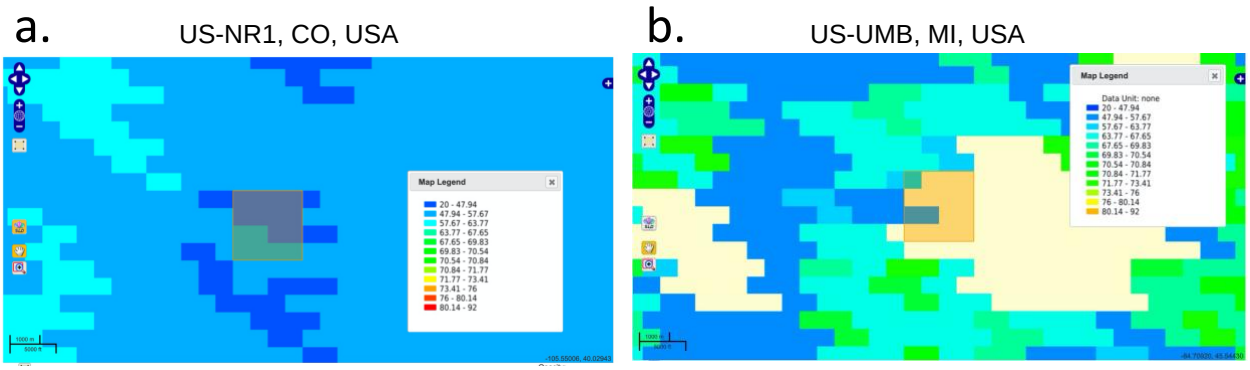

Figure S11. Spatial distribution of MODIS clumping index (He et al., 2012) over **a.** Niwot Ridge, CO, USA (center of ~2x2 km^2 box at 40.03°N, 105.55°W, 3050 m elevation), and **b.** University of Michigan Biological Station, MI, USA (center of ~2x2 km^2 box at 45.58°N, 84.72°W, 234 m elevation). Image from https://webmap.ornl.gov/ogc/dataset.jsp?ds_id=1531 (accessed on April, 28th 2021).

References

He, L., Chen, J.M., Pisek, J., Schaaf, C.B., Strahler, A.H., 2012. Global clumping index map derived from the MODIS BRDF product. Remote Sens. Environ. 119, 118–130.

Parazoo, N.C., Magney, T., Norton, A., Raczka, B., Bacour, C., Maignan, F., Baker, I., Zhang, Y., Qiu, B., Shi, M., Macbean, N., Bowling, D.R., Burns, S.P., Blanken, P.D., Stutz, J., Grossmann, K., Frankenberg, C., 2020. Wide discrepancies in the magnitude and direction of modeled solar-induced chlorophyll fluorescence in response to light conditions. Biogeosciences 17, 3733–3755. https://doi.org/10.5194/bg-17-3733-2020